THE JOURNAL OF PHYSICAL CHEMISTRY A

Article

Cite This: J. Phys. Chem. A 2019, 123, 336−342

pubs.acs.org/JPCA

Interfacial Structure and Partitioning of Nitrate Ions in Reverse Micelles

K. Jacob Blackshaw, Meredith G. Varmecky, and Joshua D. Patterson*

Department of Molecular Biology and Chemistry, Christopher Newport University, Newport News, Virginia 23606, United States

ABSTRACT: The interfacial properties of NO_3^- were investigated using reverse micelles (RMs) in solution as proxies for sea spray aerosol (SSA) particles. By tuning the size of bis(2-ethylhexyl) sulfosuccinate sodium salt (AOT) RMs doped with NO_3^- we are able to isolate the vibrational signature of interfacial NO_3^- using infrared spectroscopy. The infrared spectrum of interfacial NO_3^- along the asymmetric-stretch coordinate (υ_3) is blue-shifted and possesses smaller peak splitting relative to NO_3^- in aqueous solution. These observations are consistent with the reduced hydrogen-bonding availability of the interfacial region within the RM aqueous interior. We show that the partitioning of NO_3^- between the interfacial and core regions of the RM interior can be determined using a linear combination of interfacial and aqueous NO_3^- spectra. By fitting the interfacial partitioning curve of NO_3^- we demonstrate a method of determining quantitative interfacial affinity ($\chi_{Interface}$) for ionic species doped within RMs.

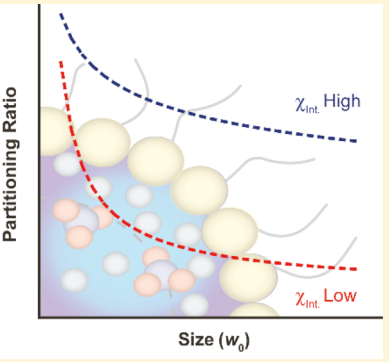

INTRODUCTION

Heterogeneous, or mixed-phase, reactions that occur in atmospheric aerosol particles are of critical importance to the atmosphere and are a crucial component of chemical reaction cycles associated with Arctic and Antarctic ozone loss, tropospheric ozone production, and acid rain.[1−27] These cycles can have serious and deleterious effects on human health. Despite the importance of heterogeneous reactions, our knowledge and ability to predict the outcomes of these reactions is limited by the complexity of the environment in which these reactions occur. Interfaces, the boundaries between chemical phases, possess unique chemical rules that cannot be described by the extension of gas- or liquid-phase properties.

In few cases are the differences in chemical properties between the interface and solution phase starker than the distribution of ions. Unlike in bulk solution, where ions are evenly distributed, ions possess intrinsic affinities toward the interfacial region. On the basis of multiple observations, interfacial affinity is dictated by a combination of charge identity (cationic vs anionic) and charge-to-size ratio.[28−58] For air−water interfaces, anions generally possess stronger relative interfacial affinities than cations and relative affinity tends to increase as charge-to-size ratio decreases. While these trends provide a framework for identifying which ions reside in the interfacial region, several studies have observed notable exceptions, in particular regarding H^+ and Mg^{2+}.[45,58] Despite the interfacial preference for anions, cationic H^+ has been observed to possess the strongest relative interfacial affinity of all ions.[45] Recent studies present an even more complex picture for Mg^{2+}, with interfacial affinity varying depending on counterion identity.[58] Mg^{2+} is located further from the interface than Cl^- and NO_3^-, consistent with interfacial affinity trends. However, when paired with SO_4^{2-}, Mg^{2+} forms solvent-shared ion pairs which orient the Mg^{2+} closer to the interface than SO_4^{2-}, an observation outside of the general interfacial trends. The sequestration of ions, such as H^+ and Mg^{2+}, to the interface over others results in concentration gradients within the interfacial region. As ions are prevalent in large concentrations in aerosol particles throughout the atmosphere,[24,25,37,59] the buildup of ions in the interfaces of aerosols could have a substantial impact on heterogeneous reactions. While general trends in relative interfacial affinity have provided new insights into the distribution of ions in the interfacial region, observed deviations from these trends have highlighted the need for quantitative descriptions of interfacial affinity and measures of the partitioning of ions between the bulk and interfacial regions. However, few quantitative descriptions of ions in the interface are currently available,[39,41,49,54,55,57] limiting our knowledge of heterogeneous reactions and ability to predict atmospheric chemistry.

In few cases is the need for quantitative descriptions of ionic distributions within interfaces more pressing than in the case of NO_3^-. Nitrate is prevalent throughout the atmosphere and is predicted to comprise up to 30% of the total particulate mass during winter.[2,60] Given the ubiquity of NO_3^- within atmospheric aerosols, numerous studies have been directed toward understanding the role NO_3^- in heterogeneous reactions cycles. NO_3^- has been identified as a product of multiple heterogeneous reactions involving nitrogen oxides (NO_x)[5,23,24,26,61] as well as a photochemical source of NO_2.[33,35,62−65] Despite these major strides in unraveling the heterogeneous chemistry of NO_3^-, deviations as large as 100% between predicted and measured wintertime NO_3^- concen-

Received: October 5, 2018
Revised: December 4, 2018
Published: December 7, 2018

DOI: 10.1021/acs.jpca.8b09751
J. Phys. Chem. A 2019, 123, 336−342

trations over the eastern United States have been observed;[2−4,66] these deviations are attributed to potentially inaccurate heterogeneous reaction rates and lack of knowledge of heterogeneous reactions as a whole. Given the importance NO_3^- in atmospheric interfaces, developing quantitative descriptions of interfacial NO_3^- is critical to reconciling experimental predictions with field observations.

Here we present an innovative and robust approach for accessing the interfacial properties of atmospherically relevant ions, using reverse micelles (RMs) in solution as proxies for marine or sea spray aerosol (SSA) particles. RMs in solution possess the same structural morphology as SSAs[67,68] as well as similar ionic conditions. Formation is achieved through the stabilization of surfactant molecules around a polar phase, in a surrounding nonpolar phase. Frequently, these structures consist of an aqueous interior or "water pool" bordered by the polar headgroups of organic surfactant molecules. The size of RMs can easily be tuned by varying the molar ratio of water to surfactant, w_0 = [H_2O]/[surfactant].[69] Interfacial studies employing RMs have previously focused on examining the dynamics and energetics of water within the RM aqueous interior.[70−91] These studies are frequently based on a core−shell or core−interfacial model to partition the aqueous interior. For a w_0 = 2 RM, all the water molecules contained within the aqueous interior are considered interfacial water, allowing for the isolation of the characteristic properties of the interfacial environment.[70−87] Interfacial H_2O is distinguished as having a unique infrared absorption spectrum, a longer vibrational lifetime, slower orientation dynamics, and a more rigid hydrogen-bonding network compared to the bulklike core H_2O.[71−85] We use bis(2-ethylhexyl) sulfosuccinate sodium salt (AOT) RMs doped with $NaNO_3$ as a platform for examining the structural properties and distribution of interfacial NO_3^-. The use of w_0 = 2 RMs allows for the isolation of the infrared spectrum of interfacial NO_3^-, which is distinct from that of aqueous NO_3^-. Vibrational band shape analysis provides information about the local hydrogen-bonding environment of the interfacial region and the bonding structure of interfacial NO_3^-. Interfacial and aqueous NO_3^- infrared absorption spectra are used to quantify the partitioning of NO_3^- between the interfacial and core regions of the RM aqueous interior. From the interfacial partitioning curve we derive a quantitative expression of interfacial affinity.

EXPERIMENTAL METHODS

Materials. AOT (Alfa Aesar, 96%) was purified according to previously described methods. Briefly, AOT was dissolved in methanol and stirred overnight with activated charcoal. The solution was then filtered, and the methanol was removed by rotary evaporation. $NaNO_3$ (Alfa Aesar, 99.0%), chloroform (Alfa Aesar, 99.8+%), and isooctane (Alfa Aesar, 99.7%) were used without additional purification. Deionized water (18 MΩ) was used for aqueous sample preparation.

Reverse Micelle Preparation. The 0.5 M AOT stock solutions were prepared in 5:1 chloroform/isooctane mixture. Undoped RMs were prepared by adding the appropriate amount of water to the AOT solution based on the desired w_0 ratio. Nitrate-doped RMs were prepared by adding an equivalent aqueous volume of 2 M $NaNO_3$ solution to the AOT stock solutions. Doped and undoped RM samples were vortexed and sonicated prior to use.

IR Characterization. IR spectroscopy measurements were conducted using a Varian 800 FT-IR. RM samples were placed in an adjustable path length cell equipped with 50−100 μm Teflon spacers and CaF_2 windows. Reported spectra were collected based on 32 scans from 1000 to 2500 cm^{-1} at a 2 cm^{-1} resolution. To isolate NO_3^- vibrational signatures, spectral contributions from the water, AOT, and the chloroform/isooctane solution were removed by subtracting the undoped RM spectrum from the nitrate-doped spectrum for equivalent w_0 ratios. Isolated NO_3^- spectra were then processed in GRAMS/AI (Thermo Scientific) using a Savitzky−Golay filter. Interfacial and core NO_3^- spectra were fit to two Gaussian functions. Interfacial−core partitioning ratios were determined by fitting NO_3^- spectra for w_0 = 4−30 to a linear combination of interfacial and core NO_3^- spectra and minimizing the residuals.

RESULTS AND DISCUSSION

The bonding structure and symmetry of NO_3^- are known to be responsive to changes in local environment. Isolated NO_3^- is planar with three equivalent N−O bonds and D_{3h} symmetry. In this symmetry the infrared-active asymmetric stretch (υ_3) is composed of two degenerate vibrations. However, interactions in condensed phases can render the N−O bonds inequivalent and break the D_{3h} symmetry. The reduction in symmetry also breaks the degeneracy of (υ_3), resulting in two distinct vibrational bands (υ_3' and υ_3'').[92] The normalized infrared spectra of the asymmetric-stretch vibrational mode (υ_3) of NO_3^- within w_0 = 2 AOT RMs and in aqueous solution are shown in Figure 1. The infrared spectrum of NO_3^- in the w_0 = 2 RM is blue-shifted and narrower relative to aqueous NO_3^-,

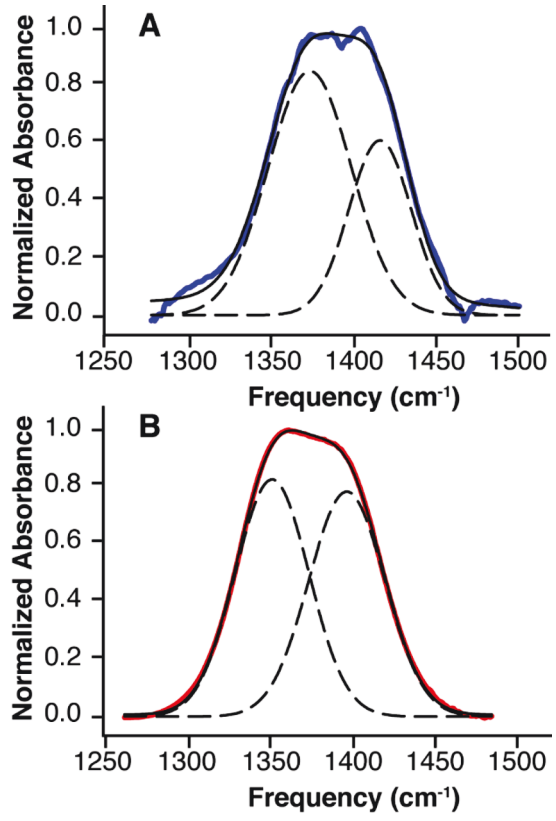

Figure 1. Normalized IR absorption spectrum of the asymmetric stretch (υ_3) of NO_3^- in (A) w_0 = 2 AOT RM (blue line) and (B) aqueous solution (red line). Spectral fits (black line) and underlying Gaussian peaks (dashed lines), corresponding to υ_3' and υ_3''.

DOI: 10.1021/acs.jpca.8b09751
J. Phys. Chem. A 2019, 123, 336−342

indicating the presences of a substantially modified form of NO_3^-, which we identify as interfacial NO_3^-. To further examine the differences between the aqueous and interfacial forms of NO_3^- the asymmetric-stretch vibrational modes (υ_3) of aqueous (core) and w_0 = 2 RM (interfacial) NO_3^- were fit to two Gaussian functions. Identification of the individual band frequencies and quantification of the extent of splitting between υ_3' and ν_3'' provide details about the local environment and bonding structure of NO_3^-. The resulting infrared absorption band frequencies, full width at half-maxima (fwhm), and frequency splitting are displayed in Table 1.

Table 1. IR Absorption Frequencies of the Nitrate Asymmetric-Stretch Vibrational Mode (υ_3), Transition Widths (fwhm), and Splitting ($\Delta\upsilon_3$) in the Core and Interfacial Regions of AOT RMs (in cm^{-1})

	υ_3'	fwhm	υ_3''	fwhm	$\Delta\upsilon_3$
core ($NO_3^-(aq)$)	1348	58	1399	58	51
interfacial (w_0 = 2)	1375	59	1417	44	42

For core NO_3^- the individual frequency bands (υ_3' and ν_3'') are located at 1348 and 1399 cm^{-1}, respectively, with identical fwhm of 58 cm^{-1}. The observed band locations and fwhm are consistent with previous studies of aqueous NO_3^-. In the case of interfacial NO_3^-, υ_3' and ν_3'' are shifted to 1375 and 1417 cm^{-1}, with corresponding fwhm of 59 and 44 cm^{-1}, respectively. In addition, the frequency splitting decreases from 51 cm^{-1} for core NO_3^- to 42 cm^{-1} for interfacial NO_3^-.

The observed differences in infrared absorption spectra between core and interfacial NO_3^- indicate substantially different local environments and bonding structures between the two forms of NO_3^-. The overall blue shift of the vibrational mode suggests a reduction in the N−O bond length from core to interfacial NO_3^-. The infrared absorption spectrum of interfacial HOD in AOT RMs has previously been observed to blue shift relative to core HOD.[76,77,79,81,85,86] The similar blue-shift responses relative to their core counterparts for interfacial NO_3^- and HOD would suggest comparable local environments and shortened bond lengths. While the line width of υ_3' remains relatively unchanged between the core and interfacial environments, ν_3'' shows a 14 cm^{-1} reduction in line width for interfacial NO_3^-. Reductions in line width are typically attributed to decreased heterogeneity of the local environment or an increase in vibrational lifetime. One of the defining characteristics of the interfacial region in RMs is an increased vibrational lifetime relative to the core.[71−77,79−85] Similar increases in vibrational lifetime and reorientation dynamics over the bulk have also been observed for solvation shell waters in solution.[83,93−96] In both cases the changes in solvent dynamics were interpreted as manifestations of the rigid of the hydrogen-bonding network. The rigidity of the hydrogen-bonding network in the interfacial region may in turn limit the ability of NO_3^- to distribute vibrational energy into local solvent modes.[94]

In addition to the band frequencies and line widths, the extent of frequency splitting of the asymmetric stretch provides several important details about the interfacial environment. Previous experimental and computational studies have determined that the frequency splitting ($\Delta\upsilon_3$) is sensitive to counterion identity and binding in solids, the strength of binding to solvents, the number of hydrogen-bonding partners, and modification N−O bond lengths.[47,93,97,98] Thøgersen et al. examined frequency splitting as a function of $\Delta G°$ for the solvent binding reaction $NO_3^- + X \rightarrow [NO_3X]^-$, noting that splitting decreased as the strength of the binding to solvent decreased.[93] The observed decrease in frequency splitting for interfacial NO_3^- relative to core NO_3^- indicates a reduction in the strength of solvent binding. As water is the solvent in both forms of NO_3^- this decrease in solvent binding strength may be indicative of reduced hydrogen-bonding interactions for interfacial NO_3^-. In addition to a decrease in the number of hydrogen-bonding interactions, the time scale of hydrogen-bond exchange may also be altered. Previous studies of aqueous NO_3^- have suggested that the solvation shell is labile and hydrogen bonds with the solvating H_2O molecules can be freely exchanged on a <2 ps time scale.[93,94] However, solvent dynamics of the interfacial region in AOT RMs are notably slower than bulk solution, occurring on an 18 ps time scale compared to 2 ps in bulk water.[81] The slow solvent dynamics and rigid hydrogen-bonding network of the interfacial region are likely to decrease the availability of hydrogen-bonding partners and increase the time scale between hydrogen-bonding events. Since frequency splitting is a direct consequence of symmetry breaking due to hydrogen-bonding interactions in water, any reduction in frequency splitting suggests that the symmetry of NO_3^- is becoming closer to D_{3h}. Decreases in frequency splitting have been linked to decreases in the root-mean-square difference of the three N−O bond lengths,[98] which further supports a reduction in hydrogen-bonding partners for interfacial NO_3^-. Taken together, the blue-shifted infrared absorption spectrum, reduced vibrational line width for ν_3'', and decreased frequency splitting ($\Delta\upsilon_3$) for w_0 = 2 NO_3^- relative to aqueous NO_3^- suggest that w_0 = 2 NO_3^- is located in an environment where hydrogen-bonding availability is limited and vibrational relaxation rates are reduced. These observations mirror the characteristics of the interfacial region and support the assignment of the infrared absorption for w_0 = 2 NO_3^- to interfacial NO_3^-. In addition, the blue-shifted infrared absorption spectrum and decreased frequency splitting indicate that interfacial NO_3^- possess shorter N−O bond lengths and that the differences in individual N−O bond lengths are reduced relative to the bonding structure of NO_3^- in bulk water.

Identification of the asymmetric-stretch vibrational mode frequencies of interfacial and core NO_3^- allows for the quantitative determination of the contributions of each form of NO_3^- to the observed infrared absorption spectra for w_0 > 2 RMs. Figure 2 shows the fit of a w_0 = 8 RM infrared absorption spectrum to a linear combination of core and interfacial NO_3^- spectra. The fit is able to reproduce the observed spectrum using an interfacial−core partitioning of 0.68 interfacial NO_3^- and 0.32 core NO_3^-, indicating that both forms of NO_3^- are present in the aqueous interior of the RM. Figure 3 displays the calculated interfacial−core partitioning of NO_3^- over the RM size progression of w_0 = 2−30. The interfacial partitioning ratio decreases steadily from 1.0 at w_0 = 2 to ∼0.25 at w_0 = 25, after which the partitioning remains relatively constant. For large RMs up to 25% of all NO_3^- contained within the water pool qualifies as interfacial and resides in close proximity to the sulfonate headgroups of AOT. Interfacial partitioning ($P_{\text{Interfacial}}$) as a function of w_0 is well-characterized by eq 1

$$P_{\text{Interfacial}} = A(w_0)^{(\chi_{\text{Interface}}-1)} \quad (1)$$

DOI: 10.1021/acs.jpca.8b09751
J. Phys. Chem. A 2019, 123, 336−342

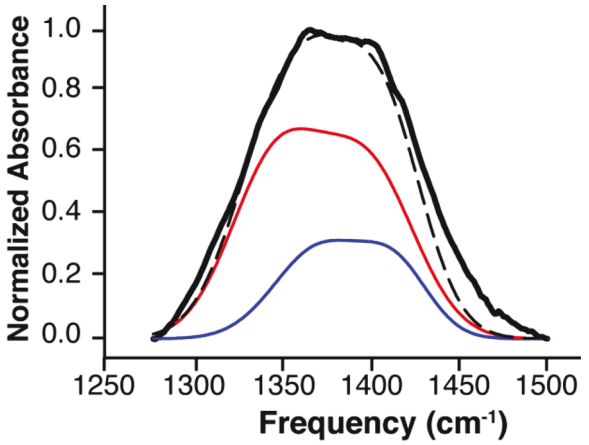

Figure 2. Normalized IR absorption spectrum of the asymmetric stretch (υ_3) of 2 M NO_3^- in a w_0 = 8 AOT RM (solid black line) and fit (dashed black line) based on the contributions of interfacial NO_3^- (blue line) and core NO_3^- (red line).

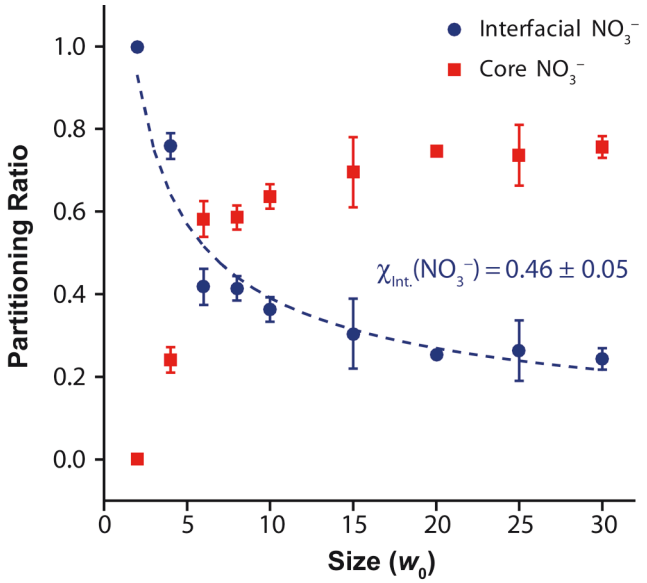

Figure 3. Interfacial–core partitioning of NO_3^- within AOT RMs based on spectral fitting using a linear combination of interfacial and core NO_3^- IR spectra. The interfacial partitioning curve is fit to the eq 1.

where $\chi_{Interface}$ is defined as the interfacial affinity and A is a prefactor. This equation places interfacial affinity on an easily interpretable scale from 1.0 to 0 with each representing the highest and lowest possible interfacial affinities, respectively. For NO_3^- in AOT RMs, $\chi_{Interface}$ = 0.46 ± 0.05 and A = 1.4 ± 0.2. While NO_3^- is expect to have a fairly strong interfacial affinity based on previous studies,[33,39,44,56,99] the negative charge of the AOT sulfonate ($R-SO_3^-$) headgroups that define the outer edge of the interfacial region is likely to suppress some NO_3^- allocation to the interfacial region. Previous studies have observed modifications of interfacial affinity due to presence of surfactant molecules.[40,41,54] While Na^+, the cationic counterion to both $R-SO_3^-$ and NO_3^- in these experiments, is believed to possess a smaller relative interfacial affinity compared to NO_3^-, electrostatic interactions likely force some of the Na^+ ions to allocate between the $R-SO_3^-$'s and NO_3^- in a multilayered ion distribution within the interfacial region. Paired charge layering concerns may therefore lower the interfacial partitioning of NO_3^-, relative to observations in bare air–water interfaces. The blue-shifted infrared spectrum of interfacial NO_3^- relative to core NO_3^- suggests that the Na^+ ions located between the $R-SO_3^-$'s and NO_3^- provide incomplete charge screening between the two anionic species. Electrostatic repulsion between the two anionic species causes NO_3^- to contract, shortening N–O bonds and resulting in a corresponding blue-shifted infrared spectrum relative to core NO_3^-, which is not subject to these electrostatic interactions. These observations raise important questions regarding ionic charge layering within the interfacial region and interfacial affinity. While previous studies have observed multilayered ion distributions within mixed ion systems,[33,35,37,45] the role interfacial affinity plays in dictating the formation of ion layers beyond a standard double layer arrangement remains unclear.

CONCLUSIONS

RMs in solution offer a powerful tool for investigating the interfacial properties of atmospherically relevant ions. The ability to isolate the signatures of interfacial species allows for the determination of interfacial–core partitioning ratios and the quantitation of interfacial affinities. On the basis of its infrared absorption spectrum, interfacial NO_3^- is more symmetric and possesses shorter N–O bond lengths compared to its core NO_3^- counterpart. These observations reflect both the slower dynamics of the local hydrogen-bonding environment as well as the complex electrostatics of the interfacial region. The distinctions between interfacial and core NO_3^- ions provided a framework for quantitatively determining the interfacial affinity. Experiments are currently underway to quantify interfacial affinity for other ionic species. Overall, quantitative interfacial affinity represents a new and vital tool for describing ionic distributions within the interfaces as well as the forces that direct the formation of ionic layering. This approach adds a new complement to existing experimental and computational techniques directed at understanding the distribution of ions in complex interfacial environments and furthering our knowledge of heterogeneous chemistry, ionic distributions, and reactive availabilities.

AUTHOR INFORMATION

Corresponding Author

*E-mail: joshua.patterson@cnu.edu.

ORCID

Joshua D. Patterson: 0000-0002-5224-0044

Notes

The authors declare no competing financial interest.

ACKNOWLEDGMENTS

This research was supported by the National Science Foundation (CHE-1708635). We thank the Christopher Newport University Summer Scholars Program for student support.

REFERENCES

(1) Alexander, B.; Hastings, M. G.; Allman, D. J.; Dachs, J.; Thornton, J. A.; Kunasek, S. A. Quantifying Atmospheric Nitrate Formation Pathways Based on a Global Model of the Oxygen Isotopic Composition ($D^{17}O$) of Atmospheric Nitrate. *Atmos. Chem. Phys.* **2009**, *9*, 5043–5056.

DOI: 10.1021/acs.jpca.8b09751
J. Phys. Chem. A 2019, 123, 336–342

(2) Heald, C. L.; Collett, J. L., Jr; Lee, T.; Benedict, K. B.; Schwandner, F. M.; Li, Y.; Clarisse, L.; Hurtmans, D. R.; Van Damme, M.; Clerbaux, C.; Coheur, P. F.; Philip, S.; Martin, R. V.; Pye, H. O. T. Atmospheric Ammonia and Particulate Inorganic Nitrogen Over the United States. *Atmos. Chem. Phys.* **2012**, *12*, 10295−10312.
(3) Sarwar, G.; Simon, H.; Bhave, P.; Yarwood, G. Examining the Impact of Heterogeneous Nitryl Chloride Production on Air Quality Across the United States. *Atmos. Chem. Phys.* **2012**, *12*, 6455−6473.
(4) Zhang, Q.; Jimenez, J. L.; Canagaratna, M. R.; Allan, J. D.; Coe, H.; Ulbrich, I.; Alfarra, M. R.; Takami, A.; Middlebrook, A. M.; Sun, Y. L.; et al. Ubiquity and Dominance of Oxygenated Species in Organic Aerosols in Anthropogenically-Influenced Northern Hemisphere Midlatitudes. *Geophys. Res. Lett.* **2007**, *34*, L1380.
(5) Bertram, T. H.; Thornton, J. A. Toward a General Parameterization of N_2O_5 Reactivity on Aqueous Particles: the Competing Effects of Particle Liquid, Water, Nitrate, and Chloride. *Atmos. Chem. Phys.* **2009**, *9*, 8351−8363.
(6) Donaldson, D. J.; Valsaraj, K. T. Adsorption and Reaction of Trace Gas-Phase Organic Compounds on Atmospheric Water Film Surfaces: A Critical Review. *Environ. Sci. Technol.* **2010**, *44*, 865−873.
(7) Dubowski, Y.; Vieceli, J.; Tobias, D. J.; Gomez, A.; Lin, A.; Nizkorodov, S. A.; McIntire, T. M.; Finlayson-Pitts, B. J. Interaction of Gas-Phase Ozone at 296 K with Unsaturated Self-Assembled Monolayers: A New Look at an Old System. *J. Phys. Chem. A* **2004**, *108*, 10473−10485.
(8) Gaston, C. J.; Thornton, J. A. Reacto-Diffusive Length of N_2O_5 in Aqueous Sulfate- and Chloride-Containing Aerosol Particles. *J. Phys. Chem. A* **2016**, *120*, 1039−1045.
(9) Kercher, J. P.; Riedel, T. P.; Thornton, J. A. Chlorine Activation by N2O5: Simultaneous, In Situ Detection of $ClNO_2$ and N_2O_5 by Chemical Ionization Mass Spectrometry. *Atmos. Meas. Tech.* **2009**, *2*, 193−204.
(10) Knipping, E. M.; Lakin, M. J.; Foster, K. L.; Jungwirth, P.; Tobias, D. J.; Gerber, R. B.; Dabdub, D.; Finlayson-Pitts, B. J. Experiments and Simulations of Ion-Enhanced Interfacial Chemistry on Aqueous NaCl Aerosols. *Science* **2000**, *288*, 301−306.
(11) McIntire, T. M.; Ryder, O.; Finlayson-Pitts, B. J. Secondary Ozonide Formation from the Ozone Oxidation of Unsaturated Self-Assembled Monolayers on Zinc Selenide Attenuated Total Reflectance Crystals. *J. Phys. Chem. C* **2009**, *113*, 11060−11065.
(12) McIntire, T. M.; Ryder, O. S.; Gassman, P. L.; Zhu, Z.; Ghosal, S.; Finlayson-Pitts, B. J. Why Ozonolysis May Not Increase the Hydrophilicity of Particles. *Atmos. Environ.* **2010**, *44*, 939−944.
(13) McNeill, V. F.; Patterson, J.; Wolfe, G. M.; Thornton, J. A. The Effect of Varying Levels of Surfactant on the Reactive Uptake of N_2O_5 to Aqueous Aerosol. *Atmos. Chem. Phys.* **2006**, *6*, 1635−1644.
(14) Mentel, T. F.; Sohn, M.; Wahner, A. Nitrate Effect in the Heterogeneous Hydrolysis of Dinitrogen Pentoxide on Aqueous Aerosols. *Phys. Chem. Chem. Phys.* **1999**, *1*, 5451−5457.
(15) Raff, J. D.; Njegic, B.; Chang, W. L.; Gordon, M. S.; Dabdub, D.; Gerber, R. B.; Finlayson-Pitts, B. J. Chlorine Activation Indoors and Outdoors via Surface-Mediated Reactions of Nitrogen Oxides with Hydrogen Chloride. *Proc. Natl. Acad. Sci. U. S. A.* **2009**, *106*, 13647−13654.
(16) Rubasinghege, G.; Grassian, V. H. Surface-Catalyzed Chlorine and Nitrogen Activation: Mechanisms for Heterogeneous Formation of ClNO, NO, NO_2, HONO, and N_2O from HNO_3 and HCl on Aluminum Oxide Particle Surfaces. *J. Phys. Chem. A* **2012**, *116*, 5180−5192.
(17) Rudich, Y. Laboratory Perspectives on the Chemical Transformations of Organic Matter in Atmospheric Particles. *Chem. Rev.* **2003**, *103*, 5097−5124.
(18) Spicer, C. W.; Chapman, E. G.; Finlayson-Pitts, B. J.; Plastridge, R. A.; Hubbe, J. M.; Fast, J. D.; Berkowitz, C. M. Unexpectedly High Concentrations of Molecular Chlorine in Coastal Air. *Nature* **1998**, *394*, 353−356.
(19) Thornton, J. A.; Abbatt, J. P. D. N_2O_5 Reaction on Submicron Sea Salt Aerosol: Kinetics, Products, and the Effect of Surface Active Organics. *J. Phys. Chem. A* **2005**, *109*, 10004−10012.
(20) Thornton, J. A.; Kercher, J. P.; Riedel, T. P.; Wagner, N. L.; Cozic, J.; Holloway, J. S.; Dube, W. P.; Wolfe, G. M.; Quinn, P. K.; Middlebrook, A. M.; et al. A Large Atomic Chlorine Source Inferred from Mid-Continental Reactive Nitrogen Chemistry. *Nature* **2010**, *464*, 271−274.
(21) Vieceli, J.; Ma, O. L.; Tobias, D. J. Uptake and Collision Dynamics of Gas Phase Ozone at Unsaturated Organic Interfaces. *J. Phys. Chem. A* **2004**, *108*, 5806−5814.
(22) Wadia, Y.; Tobias, D. J.; Stafford, R.; Finlayson-Pitts, B. J. Real-Time Monitoring of the Kinetics and Gas-Phase Products of the Reaction of Ozone with an Unsaturated Phospholipid at the Air−Water Interface. *Langmuir* **2000**, *16*, 9321−9330.
(23) Wahner, A.; Mentel, T. F.; Sohn, M.; Stier, J. Heterogeneous Reaction of N_2O_5 on Sodium Nitrate Aerosol. *J. Geophys. Res.-Atmos.* **1998**, *103*, 31103−31112.
(24) Finlayon-Pitts, B. J.; Pitts, J. N. *Chemistry in the Upper and Lower Atmosphere*; Academic Press: New York, 2000.
(25) Finlayson-Pitts, B. J. The Tropospheric Chemistry of Sea Salt: A Molecular-Level View of the Chemistry of NaCl and NaBr. *Chem. Rev.* **2003**, *103*, 4801−4822.
(26) Finlayson-Pitts, B. J. Reactions at Surfaces in the Atmosphere: Integration of Experiments and Theory as Necessary (But Not Necessarily Sufficient) for Predicting the Physical Chemistry of Aerosols. *Phys. Chem. Chem. Phys.* **2009**, *11*, 7760−7779.
(27) Finlayson-Pitts, B. J.; Wingen, L. M.; Sumner, A. L.; Syomin, D.; Ramazan, K. A. The Heterogeneous Hydrolysis of NO_2 in Laboratory Systems and in Outdoor and Indoor Atmospheres: An Integrated Mechanism. *Phys. Chem. Chem. Phys.* **2003**, *5*, 223−242.
(28) Jungwirth, P.; Finlayson-Pitts, B. J.; Tobias, D. J. Introduction: Structure and Chemistry at Aqueous Interfaces. *Chem. Rev.* **2006**, *106*, 1137−1139.
(29) Jungwirth, P.; Tobias, D. J. Molecular Structure of Salt Solutions: A New View of the Interface with Implications for Heterogeneous Atmospheric Chemistry. *J. Phys. Chem. B* **2001**, *105*, 10468−10472.
(30) Jungwirth, P.; Tobias, D. J. Ions at the Air/Water Interface. *J. Phys. Chem. B* **2002**, *106*, 6361−6373.
(31) Jungwirth, P.; Tobias, D. J. Specific Ion Effects at the Air/Water Interface. *Chem. Rev.* **2006**, *106*, 1259−1281.
(32) Mucha, M.; Frigato, T.; Levering, L. M.; Allen, H. C.; Tobias, D. J.; Dang, L. X.; Jungwirth, P. Unified Molecular Picture of the Surfaces of Aqueous Acid, Base, and Salt Solutions. *J. Phys. Chem. B* **2005**, *109*, 7617−7623.
(33) Richards, N. K.; Wingen, L. M.; Callahan, K. M.; Nishino, N.; Kleinman, M. T.; Tobias, D. J.; Finlayson-Pitts, B. J. Nitrate Ion Photolysis in Thin Water Films in the Presence of Bromide Ions. *J. Phys. Chem. A* **2011**, *115*, 5810−5821.
(34) Tobias, D. J.; Hemminger, J. C. Getting Specific About Specific Ion Effects. *Science* **2008**, *319*, 1197−1198.
(35) Wingen, L. M.; Moskun, A. C.; Johnson, S. N.; Thomas, J. L.; Roeselova, M.; Tobias, D. J.; Kleinman, M. T.; Finlayson-Pitts, B. J. Enhanced surface photochemistry in chloride-nitrate ion mixtures. *Phys. Chem. Chem. Phys.* **2008**, *10*, 5668−5677.
(36) Allen, H. C.; Casillas-Ituarte, N. N.; Sierra-Hernandez, M. R.; Chen, X.; Tang, C. Y. Shedding Light on Water Structure at Air-Aqueous Interfaces: Ions, Lipids, and Hydration. *Phys. Chem. Chem. Phys.* **2009**, *11*, 5538−5549.
(37) Ault, A. P.; Guasco, T. L.; Ryder, O. S.; Baltrusaitis, J.; Cuadra-Rodriguez, L. A.; Collins, D. B.; Ruppel, M. J.; Bertram, T. H.; Prather, K. A.; Grassian, V. H. Inside versus Outside: Ion Redistribution in Nitric Acid Reacted Sea Spray Aerosol Particles as Determined by Single Particle Analysis. *J. Am. Chem. Soc.* **2013**, *135*, 14528−14531.
(38) Ault, A. P.; Zhao, D.; Ebben, C. J.; Tauber, M. J.; Geiger, F. M.; Prather, K. A.; Grassian, V. H. Raman microspectroscopy and Vibrational Sum Frequency Generation Spectroscopy as Probes of the Bulk and Surface Compositions of Size-Resolved Sea Spray Aerosol Particles. *Phys. Chem. Chem. Phys.* **2013**, *15*, 6206−6214.

DOI: 10.1021/acs.jpca.8b09751
J. Phys. Chem. A 2019, 123, 336−342

(39) Brown, M. A.; Winter, B.; Faubel, M.; Hemminger, J. C. Spatial Distribution of Nitrate and Nitrite Anions at the Liquid/Vapor Interface of Aqueous Solutions. *J. Am. Chem. Soc.* **2009**, *131*, 8354−8355.
(40) Casper, C. B.; Verreault, D.; Adams, E. M.; Hua, W.; Allen, H. C. Surface Potential of DPPC Monolayers on Concentrated Aqueous Salt Solutions. *J. Phys. Chem. B* **2016**, *120*, 2043−2052.
(41) Cheng, J.; Vecitis, C. D.; Hoffmann, M. R.; Colussi, A. J. Experimental Anion Affinities for the Air/Water Interface. *J. Phys. Chem. B* **2006**, *110*, 25598−25602.
(42) Gopalakrishnan, S.; Jungwirth, P.; Tobias, D. J.; Allen, H. C. Air−Liquid Interfaces of Aqueous Solutions Containing Ammonium and Sulfate: Spectroscopic and Molecular Dynamics Studies. *J. Phys. Chem. B* **2005**, *109*, 8861−8872.
(43) Hua, W.; Chen, X.; Allen, H. C. Phase-Sensitive Sum Frequency Revealing Accommodation of Bicarbonate Ions, and Charge Separation of Sodium and Carbonate Ions within the Air/Water Interface. *J. Phys. Chem. A* **2011**, *115*, 6233−6238.
(44) Hua, W.; Verreault, D.; Allen, H. C. Surface Electric Fields of Aqueous Solutions of NH4NO3, $Mg(NO_3)_2$, $NaNO_3$, and $LiNO_3$: Implications for Atmospheric Aerosol Chemistry. *J. Phys. Chem. C* **2014**, *118*, 24941−24949.
(45) Hua, W.; Verreault, D.; Allen, H. C. Relative Order of Sulfuric Acid, Bisulfate, Hydronium, and Cations at the Air−Water Interface. *J. Am. Chem. Soc.* **2015**, *137*, 13920−13926.
(46) Hua, W.; Verreault, D.; Huang, Z.; Adams, E. M.; Allen, H. C. Cation Effects on Interfacial Water Organization of Aqueous Chloride Solutions. I. Monovalent Cations: Li^+, Na^+, K^+, and NH_4^+. *J. Phys. Chem. B* **2014**, *118*, 8433−8440.
(47) Hudson, P. K.; Schwarz, J.; Baltrusaitis, J.; Gibson, E. R.; Grassian, V. H. A Spectroscopic Study of Atmospherically Relevant Concentrated Aqueous Nitrate Solutions. *J. Phys. Chem. A* **2007**, *111*, 544−548.
(48) Krisch, M. J.; D'Auria, R.; Brown, M. A.; Tobias, D. J.; Hemminger, C.; Ammann, M.; Starr, D. E.; Bluhm, H. The Effect of an Organic Surfactant on the Liquid−Vapor Interface of an Electrolyte Solution. *J. Phys. Chem. C* **2007**, *111*, 13497−13509.
(49) Pegram, L. M.; Record, M. T. Partitioning of Atmospherically Relevant Ions Between Bulk Water and the Water/Vapor Interface. *Proc. Natl. Acad. Sci. U. S. A.* **2006**, *103*, 14278−14281.
(50) Petersen, P. B.; Saykally, R. J. Probing the Interfacial Structure of Aqueous Electrolytes with Femtosecond Second Harmonic Generation Spectroscopy. *J. Phys. Chem. B* **2006**, *110*, 14060−14073.
(51) Richmond, G. L. Molecular Bonding and Interactions at Aqueous Surfaces as Probed by Vibrational Sum Frequency Spectroscopy. *Chem. Rev.* **2002**, *102*, 2693−2724.
(52) Tang, C. Y.; Allen, H. C. Ionic Binding of Na^+ versus K^+ to the Carboxylic Acid Headgroup of Palmitic Acid Monolayers Studied by Vibrational Sum Frequency Generation Spectroscopy. *J. Phys. Chem. A* **2009**, *113*, 7383−7393.
(53) Tian, C.; Byrnes, S. J.; Han, H.-L.; Shen, Y. R. Surface Propensities of Atmospherically Relevant Ions in Salt Solutions Revealed by Phase-Sensitive Sum Frequency Vibrational Spectroscopy. *J. Phys. Chem. Lett.* **2011**, *2*, 1946−1949.
(54) Wen, Y.-C.; Zha, S.; Tian, C.; Shen, Y. R. Surface pH and Ion Affinity at the Alcohol-Monolayer/Water Interface Studied by Sum-Frequency Spectroscopy. *J. Phys. Chem. C* **2016**, *120*, 15224−15229.
(55) Wren, S. N.; Donaldson, D. J. Glancing-Angle Raman Study of Nitrate and Nitric acid at the Air−Aqueous Interface. *Chem. Phys. Lett.* **2012**, *522*, 1−10.
(56) Xu, M.; Tang, C. Y.; Jubb, A. M.; Chen, X.; Allen, H. C. Nitrate Anions and Ion Pairing at the Air−Aqueous Interface†. *J. Phys. Chem. C* **2009**, *113*, 2082−2087.
(57) Yamaguchi, S.; Bhattacharyya, K.; Tahara, T. Acid−Base Equilibrium at an Aqueous Interface: pH Spectrometry by Heterodyne-Detected Electronic Sum Frequency Generation. *J. Phys. Chem. C* **2011**, *115*, 4168−4173.
(58) Götte, L.; Parry, K. M.; Hua, W.; Verreault, D.; Allen, H. C.; Tobias, D. J. Solvent-Shared Ion Pairs at the Air−Solution Interface of Magnesium Chloride and Sulfate Solutions Revealed by Sum Frequency Spectroscopy and Molecular Dynamics Simulations. *J. Phys. Chem. A* **2017**, *121*, 6450−6459.
(59) Prather, K. A.; Bertram, T. H.; Grassian, V. H.; Deane, G. B.; Stokes, M. D.; DeMott, P. J.; Aluwihare, L. I.; Palenik, B. P.; Azam, F.; Seinfeld, J. H. Bringing the Ocean into the Laboratory to Probe the Chemical Complexity of Sea Spray Aerosol. *Proc. Natl. Acad. Sci. U. S. A.* **2013**, *110*, 7550−7555.
(60) Wyat Appel, K.; Bhave, P. V.; Gilliland, A. B.; Sarwar, G.; Roselle, S. J. Evaluation of the Community Multiscale Air Quality (CMAQ) Model Version 4.5: Sensitivities Impacting Model Performance; Part II—Particulate Matter. *Atmos. Environ.* **2008**, *42*, 6057−6066.
(61) Shaloski, M. A.; Gord, J. R.; Staudt, S.; Quinn, S. L.; Bertram, T. H.; Nathanson, G. M. Reactions of N_2O_5 with Salty and Surfactant-Coated Glycerol: Interfacial Conversion of Br^- to Br_2 Mediated by Alkylammonium Cations. *J. Phys. Chem. A* **2017**, *121*, 3708−3719.
(62) Karagulian, F.; Dilbeck, C. W.; Finlayson-Pitts, B. J. Unusual Oxidation of Organics at Interfaces from the Bottom Up and Atmospheric Implications. *J. Am. Chem. Soc.* **2008**, *130*, 11272−11273.
(63) Karagulian, F.; Dilbeck, C. W.; Finlayson-Pitts, B. J. Nitrite-Induced Oxidation of Organic Coatings on Models for Airborne Particles†. *J. Phys. Chem. A* **2009**, *113*, 7205−7212.
(64) Reeser, D. I.; Kwamena, N.-O. A.; Donaldson, D. J. Effect of Organic Coatings on Gas-Phase Nitrogen Dioxide Production from Aqueous Nitrate Photolysis. *J. Phys. Chem. C* **2013**, *117*, 22260−22267.
(65) Richards, N. K.; Finlayson-Pitts, B. J. Production of Gas Phase NO_2 and Halogens from the Photochemical Oxidation of Aqueous Mixtures of Sea Salt and Nitrate Ions at Room Temperature. *Environ. Sci. Technol.* **2012**, *46*, 10447−10454.
(66) Mathur, R.; Yu, S.; Kang, D.; Schere, K. L. Assessment of the Wintertime Performance of Developmental Particulate Matter Forecasts with the Eta-Community Multiscale Air Quality Modeling System. *J. Geophys. Res.* **2008**, *113*, D02303.
(67) Levinger, N. E.; Rubenstrunk, L. C.; Baruah, B.; Crans, D. C. Acidification of Reverse Micellar Nanodroplets by Atmospheric Pressure CO_2. *J. Am. Chem. Soc.* **2011**, *133*, 7205−7214.
(68) Ellison, G. B.; Tuck, A. F.; Vaida, V. Atmospheric Processing of Organic Aerosols. *J. Geophys. Res.* **1999**, *104*, 11633−11641.
(69) De, T. K.; Maitra, A. Solution Behaviour of Aerosol OT in Non-Polar Solvents. *Adv. Colloid Interface Sci.* **1995**, *59*, 95−193.
(70) Costard, R.; Levinger, N. E.; Nibbering, E. T. J.; Elsaesser, T. Ultrafast Vibrational Dynamics of Water Confined in Phospholipid Reverse Micelles. *J. Phys. Chem. B* **2012**, *116*, 5752−5759.
(71) Deàk, J. C.; Pang, Y.; Sechler, T. D.; Wang, Z.; Dlott, D. D. Vibrational Energy Transfer Across a Reverse Micelle Surfactant Layer. *Science* **2004**, *306*, 473−476.
(72) Dokter, A. M.; Woutersen, S.; Bakker, H. J. Inhomogeneous Dynamics in Confined Water Nanodroplets. *Proc. Natl. Acad. Sci. U. S. A.* **2006**, *103*, 15355−15358.
(73) Dokter, A. M.; Woutersen, S.; Bakker, H. J. Ultrafast Dynamics of Water in Cationic Micelles. *J. Chem. Phys.* **2007**, *126*, 124507.
(74) Fayer, M. D. Dynamics of Water Interacting with Interfaces, Molecules, and Ions. *Acc. Chem. Res.* **2012**, *45*, 3−14.
(75) Fenn, E. E.; Wong, D. B.; Fayer, M. D. Water Dynamics at Neutral and Ionic Interfaces. *Proc. Natl. Acad. Sci. U. S. A.* **2009**, *106*, 15243−15248.
(76) Fenn, E. E.; Wong, D. B.; Fayer, M. D. Water Dynamics in Small Reverse Micelles in Two Solvents: Two-Dimensional Infrared Vibrational Echoes with Two-Dimensional Background Subtraction. *J. Chem. Phys.* **2011**, *134*, 054512.
(77) Fenn, E. E.; Wong, D. B.; Giammanco, C. H.; Fayer, M. D. Dynamics of Water at the Interface in Reverse Micelles: Measurements of Spectral Diffusion with Two-Dimensional Infrared Vibrational Echoes. *J. Phys. Chem. B* **2011**, *115*, 11658−11670.
(78) Levinger, N. E.; Swafford, L. A. Ultrafast Dynamics in Reverse Micelles. *Annu. Rev. Phys. Chem.* **2009**, *60*, 385−406.

DOI: 10.1021/acs.jpca.8b09751
J. Phys. Chem. A 2019, 123, 336−342

(79) Moilanen, D. E.; Fenn, E. E.; Wong, D.; Fayer, M. D. Water Dynamics at the Interface in AOT Reverse Micelles. *J. Phys. Chem. B* **2009**, *113*, 8560−8568.
(80) Moilanen, D. E.; Fenn, E. E.; Wong, D.; Fayer, M. D. Geometry and Nanolength Scales versus Interface Interactions: Water Dynamics in AOT Lamellar Structures and Reverse Micelles. *J. Am. Chem. Soc.* **2009**, *131*, 8318−8328.
(81) Moilanen, D. E.; Fenn, E. E.; Wong, D.; Fayer, M. D. Water Dynamics in Large and Small Reverse Micelles: From Two Ensembles to Collective Behavior. *J. Chem. Phys.* **2009**, *131*, 014704.
(82) Moilanen, D. E.; Levinger, N. E.; Spry, D. B.; Fayer, M. D. Confinement or the Nature of the Interface? Dynamics of Nanoscopic Water. *J. Am. Chem. Soc.* **2007**, *129*, 14311−14318.
(83) Park, S.; Moilanen, D. E.; Fayer, M. D. Water Dynamics The Effects of Ions and Nanoconfinement. *J. Phys. Chem. B* **2008**, *112*, 5279−5290.
(84) Piletic, I. R.; Moilanen, D. E.; Spry, D. B.; Levinger, N. E.; Fayer, M. D. Testing the Core/Shell Model of Nanoconfined Water in Reverse Micelles Using Linear and Nonlinear IR Spectroscopy. *J. Phys. Chem. A* **2006**, *110*, 4985−4999.
(85) Piletic, I. R.; Tan, H.-S.; Fayer, M. D. Dynamics of Nanoscopic Water. *J. Phys. Chem. B* **2005**, *109*, 21273−21284.
(86) Tan, H.-S.; Piletic, I. R.; Fayer, M. D. Orientational Dynamics of Water Confined on a Nanometer Length Scale in Reverse Micelles. *J. Chem. Phys.* **2005**, *122*, 174501.
(87) Tan, H.-S.; Piletic, I. R.; Riter, R. E.; Levinger, N. E.; Fayer, M. D. Dynamics of Water Confined. *Phys. Rev. Lett.* **2005**, *94*, 057405.
(88) Corbeil, E. M.; Riter, R. E.; Levinger, N. E. Cosurfactant Impact on Probe Molecule in Reverse Micelles. *J. Phys. Chem. B* **2004**, *108*, 10777−10784.
(89) Correa, N. M.; Levinger, N. E. What Can You Learn from a Molecular Probe? New Insights on the Behavior of C343 in Homogeneous Solutions and AOT Reverse Micelles. *J. Phys. Chem. B* **2006**, *110*, 13050−13061.
(90) Riter, R. E.; Willard, D. M.; Levinger, N. E. Water Immobilization at Surfactant Interfaces in Reverse Micelles. *J. Phys. Chem. B* **1998**, *102*, 2705−2714.
(91) Sedgwick, M.; Cole, R. L.; Rithner, C. D.; Crans, D. C.; Levinger, N. E. Correlating Proton Transfer Dynamics To Probe Location in Confined Environments. *J. Am. Chem. Soc.* **2012**, *134*, 11904−11907.
(92) Ramesh, S. G.; Re, S.; Boisson, J.; Hynes, J. T. Vibrational Symmetry Breaking of NO3− in Aqueous Solution: NO Asymmetric Stretch Frequency Distribution and Mean Splitting. *J. Phys. Chem. A* **2010**, *114*, 1255−1269.
(93) Thøgersen, J.; Réhault, J.; Odelius, M.; Ogden, T.; Jena, N. K.; Jensen, S. J. K.; Keiding, S. R.; Helbing, J. Hydration Dynamics of Aqueous Nitrate. *J. Phys. Chem. B* **2013**, *117*, 3376−3388.
(94) Fournier, J. A.; Carpenter, W.; De Marco, L.; Tokmakoff, A. Interplay of Ion−Water and Water−Water Interactions within the Hydration Shells of Nitrate and Carbonate Directly Probed with 2D IR Spectroscopy. *J. Am. Chem. Soc.* **2016**, *138*, 9634−9645.
(95) Giammanco, C. H.; Wong, D. B.; Fayer, M. D. Water Dynamics in Divalent and Monovalent Concentrated Salt Solutions. *J. Phys. Chem. B* **2012**, *116*, 13781−13792.
(96) Vila Verde, A.; Lipowsky, R. Cooperative Slowdown of Water Rotation near Densely Charged Ions Is Intense but Short-Ranged. *J. Phys. Chem. B* **2013**, *117*, 10556−10566.
(97) Goebbert, D. J.; Garand, E.; Wende, T.; Bergmann, R.; Meijer, G.; Asmis, K. R.; Neumark, D. M. Infrared Spectroscopy of the Microhydrated Nitrate Ions $NO_3^-(H_2O)_{1-6}$. *J. Phys. Chem. A* **2009**, *113*, 7584−7592.
(98) Waterland, M. R.; Stockwell, D.; Kelley, A. M. Symmetry Breaking Effects in NO_3^-: Raman Spectra of Nitrate Salts and Ab Initio Resonance Raman Spectra of Nitrate−Water Complexes. *J. Chem. Phys.* **2001**, *114*, 6249−6258.
(99) Thomas, J. L.; Roeselová, M.; Dang, L. X.; Tobias, D. J. Molecular Dynamics Simulations of the Solution−Air Interface of Aqueous Sodium Nitrate. *J. Phys. Chem. A* **2007**, *111*, 3091−3098.

DOI: 10.1021/acs.jpca.8b09751
J. Phys. Chem. A 2019, 123, 336−342